Seismic Observations of Four Thunderstorms Using an Underground Fiber-Optic Array

Samuel Hone*[1] and Tieyuan Zhu[1]

Abstract

Thunderstorms are a common atmospheric phenomenon that cause abundant acoustic disturbances, which can interact with the ground surface, creating a link between atmospheric and solid Earth processes. This article reports seismological observations of four thunderstorms through the spring and summer of 2019, as recorded by the distributed acoustic sensing fiber-optic array (4.9 km) on the Penn State campus in State College, Pennsylvania. With a dense sensor array in the local region, we are able to construct the seismic full waveform response of the thunderstorm events (hereafter referred to as thunderquakes) and track the wave propagation across the array. We use a time-domain grid search to obtain the back azimuth and slowness of the waves, and a modified Geiger's method to pinpoint source locations of the thunderquakes. Correlated with the time of the recorded signal, this data allows reconstruction of thunderstorm movement as well as offering measurements of the seismic velocity.

Cite this article as Hone, S., and T. Zhu (2021). Seismic Observations of Four Thunderstorms Using an Underground Fiber-Optic Array, *Seismol. Res. Lett.* **XX**, 1–10, doi: 10.1785/0220200264.

Introduction

Thunderstorms are an extremely common occurrence in areas all over the globe, with over 2000 storms happening at any given moment, and the central and eastern United States, in particular, can experience up to 50 storm days per year according to the National Oceanic and Atmospheric Administration National Severe Storms Laboratory. A variety of hazards associated with these events, including flooding, lightning damage, wildfires, and hail, can have substantial societal impacts, damaging buildings and other infrastructure and resulting in billions of dollars of global economic loss, as well as many human injuries and fatalities. The dangers posed by thunderstorms led to the creation of a National Lightning Detection Network (NLDN) in the late 1990s (Cummins *et al.*, 1998) and the new Global Lightning Mapper (GLM) that measures total lightning activity from on board the Geostationary Operational Environmental Satellite-16 (Rudlosky *et al.*, 2019). The NLDN and the GLM are now the primary tools for lightning observations.

Thunderstorms can interact with the solid Earth via lightning stroke and/or thunder. Prior studies favor the acoustic–seismic theory that the acoustic disturbance of thunder transfers its energy to the Earth's surface, exciting seismic waves in the shallow subsurface (Kappus and Vernon, 1991; Lin and Langston, 2007). Seismic observations of these events using a dense sensor array may provide a unique opportunity to study the physical features of thunderstorms and the nature of their interactions with the solid Earth. In this study, we show that a local fiber-optic distributed acoustic sensing (DAS) array can detect seismic signals associated with lightning thunder, and can provide additional data to identify and track thunderstorm movement on a local scale.

Previous studies have shown that a variety of atmospheric disturbances, such as sonic booms, meteoroid falls, thunder, hurricanes, and explosions, produce sufficient changes in air pressure from the shock wave to induce a ground motion in the shallow subsurface (Kanamori *et al.*, 1991; Langston, 2004; Lin and Langston, 2006; Ebeling and Stein, 2011). The acoustic signature left by thunder in the seismic record was first investigated by Kappus and Vernon (1991), who used polarization analysis of three-component seismograms, to determine the particle motion induced by thunder and to analyze the lightning channel path as well as investigating mechanisms of acoustic–seismic coupling. Lin and Langston (2007) used side-by-side arrays of microphones and seismometers, to record thunder-induced ground motions (thunderquakes), and proposed the use of such signals as a viable seismic source for hazard assessments. A follow-up study by Lin and Langston (2009a) used time-domain transfer functions to examine the relationship between the acoustic wave and the ground motion, and a further study (Lin and Langston, 2009b) used thunderquakes to characterize near-surface velocity structure. Voss

1. Department of Geosciences, The Pennsylvania State University, State College, Pennsylvania, U.S.A.

*Corresponding author: svh5840@psu.edu

© Seismological Society of America

Downloaded from http://pubs.geoscienceworld.org/ssa/srl/article-pdf/doi/10.1785/0220200264/5276217/srl-2020264.1.pdf?casa_token=1-AImUXu6LMAAAAA:MKb73oRGMLD2ar73L2OqF-jelQ0EqtL7mYIlc1TycF5O5zVJmVsUHJV
by Pennsylvania State Univ Serials Dept, Tieyuan

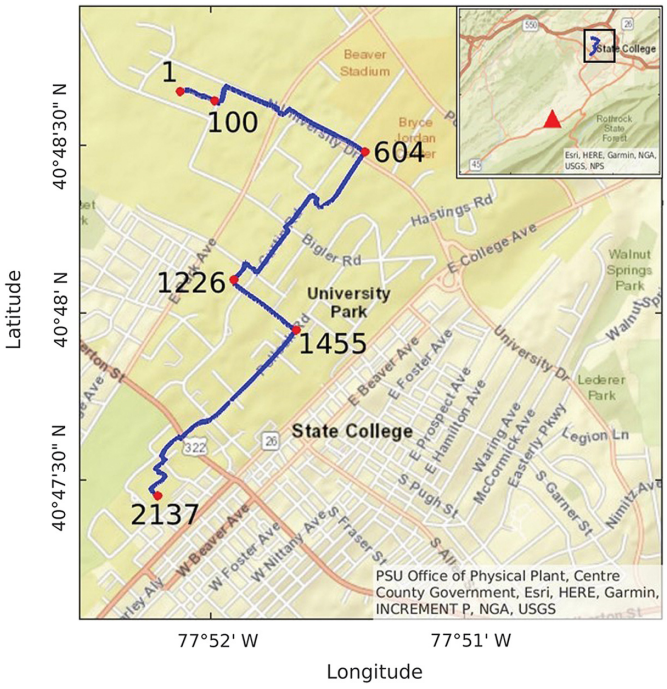


Figure 1. Location of the Fiber Optic foR Environmental SEnsEing (FORESEE) fiber-optic array underneath Penn State campus, shown in blue, with important channel numbers labeled and marked in red. The array stretches approximately 4900 m and is buried about a meter deep. In the inset, the red triangle represents the location of the PSRS seismic station, located 11 km to the southwest, which was used for signal comparison. NGA, Next Generation Attenuation; USGS, U.S. Geological Survey. The color version of this figure is available only in the electronic edition.

et al. (2015) noted the characteristics of thunderquakes and other atmospheric signals on seismometers, to distinguish them from the earthquake record.

Although past studies have used seismometers to measure thunderquakes, these observations suffer due to sparse arrays, especially in areas that experience little seismic activity, such as the eastern United States. Denser arrays improve data resolution and would enable local-scale tracking of storm progress as well as improving our understanding of the mechanisms of thunderquakes and thunderstorms.

A recent study by Zhu and Stensrud (2019) showed that a DAS fiber-optic array can effectively record signals from thunderstorms. DAS technology transforms tens of kilometers of fiber-optic cable into thousands of sensors at the meter scale. Such a spatially dense array is an excellent means to study thunderquakes, especially in urban areas where telecommunication fiber optics have been widely installed in the past decades. They reported 18 specific events detected in the data from a thunderstorm on 15 April 2019.

In this study, we present an additional 105 events from four separate thunderstorms in the summer of 2019, demonstrating that these signals are quite common and simple to detect. We demonstrate wave propagation through the array and analyze the frequency content of the events, then we use the grid-search method of Lin and Langston (2007) to determine the source azimuth and slowness, locate the source using Geiger's method (Menke, 2012), and chart the progress of the thunderstorms using the timing and location of the seismic sources.

DAS Fiber-Optic Array

This study uses continuous seismic data recorded by the DAS array that is part of the Fiber Optic foR Environmental SEnsEing (FORESEE) project on the Penn State campus in State College, Pennsylvania (Zhu *et al.*, 2021). The FORESEE array uses one strand of an existing fiber-optic telecommunications cable laid in concrete conduit about a meter below ground level. The cable is connected to a Silixa iDAS2 interrogator, which continuously measures strain rate in units of nanostrain per second at a 500 Hz sampling frequency with a 10 m gauge length. The array has a channel spacing of 2 m, for a total of 2137 channels over 4274 m, and has been in continuous operation since 5 April 2019 (Fig. 1).

The nonlinear shape of the fiber-optic array, including multiple 90° turns, allows for more accurate pinpointing of event sources, as well as aiding analysis of particle velocity direction. Similar to geophone sensing of particle velocity, DAS sensing of the strain rate shows angular sensitivity to Rayleigh and Love waves, and, because the best results appear when the wave propagation direction is parallel to the DAS array (Martin *et al.*, 2017), the shape of the array allows for good sensitivity in all directions. Combined with the dense sampling and length of the array, the shape makes it well suited for local-scale tracking of lightning events.

DAS Recordings of Thunderstorms

Data from the Penn State Climatologist website reveal that Pennsylvania experiences 30–35 severe thunderstorms per year, typically concentrated in the spring and late summer. We utilized past weather alerts and online storm records, to locate target thunderstorm dates and times for the State College area, and manually scanned the data for strong anomalies spanning the array. On four dates through the spring and summer of 2019, we identify 105 thunderquakes in the DAS data, adding to the 18 already identified on 15 April 2019, by Zhu and Stensrud (2019). Although thunderstorms were reported on other dates in this time period, some did not show strong thunderquake signals and others have yet to be investigated. The dates used are identified in Table 1, along with the approximate time spanned by each thunderstorm period based on the presence of thunderquakes in the data. The approximate direction of origin for each thunderstorm was determined independently from the DAS data by inspecting weather radar from the website available in Data and Resources.

Using thunderquakes from 18 August 2019 as an example, we show a single channel (channel 100) with 2 hr of thunderquake

Downloaded from http://pubs.geoscienceworld.org/ssa/srl/article-pdf/doi/10.1785/0220200264/5276217/srl-2020264.1.pdf?casa_token=1-AImUXu6LMAAAAA:MKb73oRGMLD2ar73L2OqF-jelQ0EqtL7mYIlc1TycF5O5zVJmVsUHJV
by Pennsylvania State Univ Serials Dept, Tieyuan

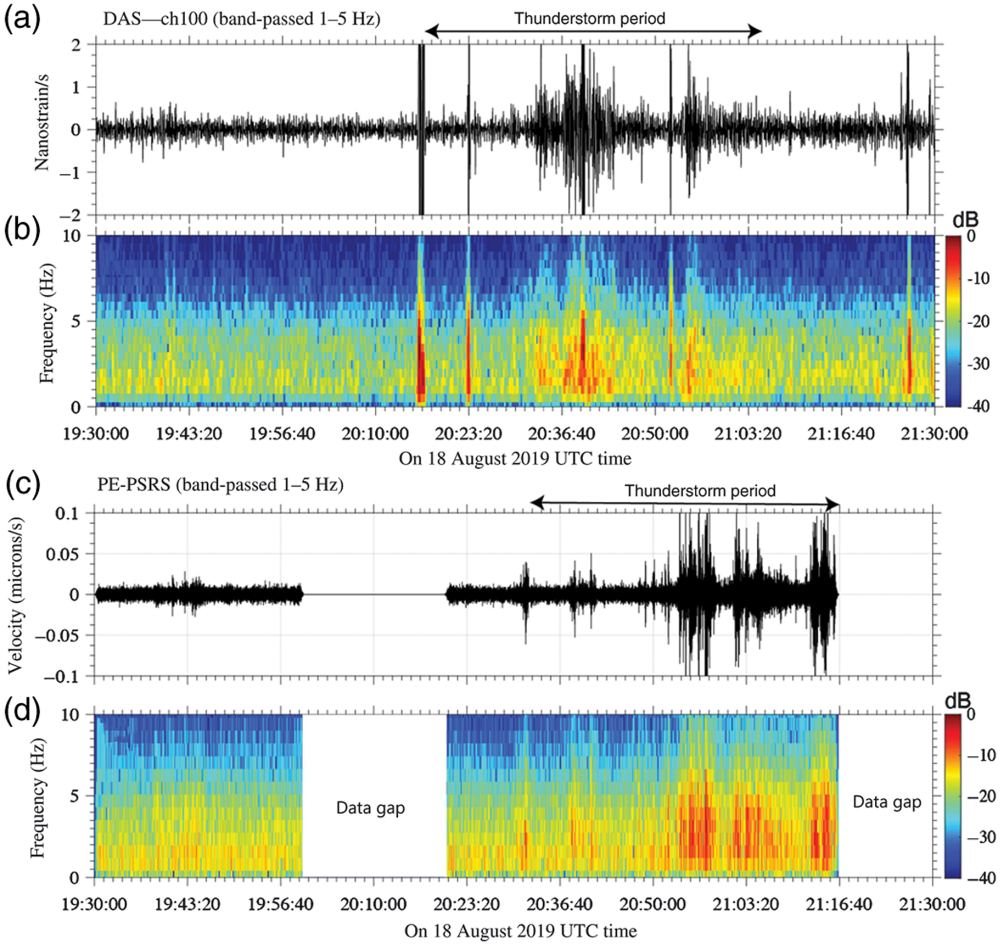


Figure 2. (a) Two hours of thunderquake (18 August 2019) waveform data by distributed acoustic sensing (DAS) measuring strain rate and (c) the nearby PSRS seismic station measuring ground velocity in the (1–5) Hz range with (b,d) their corresponding spectrograms. The seismogram shows a similar pattern of peaks but with a delay of about 10 min. The color version of this figure is available only in the electronic edition.

waveform data recorded by DAS after applying a band-pass filter (1–5) Hz in Figure 2a. In the 2 hr waveform, we found many strong waveform spikes, in particular, after 20:15 UTC, denoting strong thunderquake events. These spikes persist to about 21:00 UTC. We also compare the DAS waveform to the seismogram from the closest seismic station (PE-PSRS) located 11 km to the southwest in Figure 2c. Considering the general movement direction of thunderstorms in the area (northwest to southeast) and the location of PSRS (see Fig. 1), these delayed strong spikes in the seismogram may be registered after the thunderstorm moved to the PSRS area. Similar features can be identified on each record in the form of sharp waveforms followed by dispersion patterns. Because of the distance between the fiber array and the seismometer, however, it is not straightforward to directly match individual thunderquakes across the two records. Using the moveout of the signal visible through multiple channels, the number of thunder events identified on each date varies from 2 on 28 May to 46 on 18 August. Events were identified by first locating past thunderstorm dates in the weather record and then examining the DAS data with a broadband filter (1–200) Hz to catch the full frequency range from the thunderquakes. Recognizable event first arrivals were manually picked in MATLAB (see Data and Resources) on ~50 evenly spaced channels with an uncertainty within about 1 s and then interpolated to cover all channels.

TABLE 1
Thunderstorm Times and Movement Directions

Date and Time (yyyy/mm/dd hh:mm–hh:mm) UTC	Direction of Origin	Number of Events
2019/04/15 03:21–03:50	Southwest	18
2019/05/19 19:07–22:29	Southwest	16
2019/05/28 23:20–23:23	West	2
2019/05/29 18:57–19:58	West-southwest	40
2019/08/18 20:22–21:30	West-northwest	46

Figure 3 shows examples of the identified events from each date, plotted with all 2137 channels, and with individual traces and spectrograms. In each event, there is significant noise around channels 1000 and 1400, likely due to turning points in the array, causing a signal overlap, as well as other random noise due to local traffic, and so forth (see Fig. 3a). This does not, however, notably impede picking of first arrivals for each event, because clear first arrivals are evident in the figure. These arrivals show varying offsets, with event 61 being almost linear and the others showing a degree of kinking in the arrivals, which is likely due to the shape of the array. Events 36 and 122, in particular, show kinks in the arrivals, corresponding to major turning points in the array (see Fig. 1b,d). The linear

Downloaded from http://pubs.geoscienceworld.org/ssa/srl/article-pdf/doi/10.1785/0220200264/5276217/srl-2020264.1.pdf?casa_token=1-AImUXu6LMAAAAA:MKb73oRGMLD2ar73L2OqF-jelQ0EqtL7mYIlc1TycF5O5zVJmVsUHJV
by Pennsylvania State Univ Serials Dept, Tieyuan

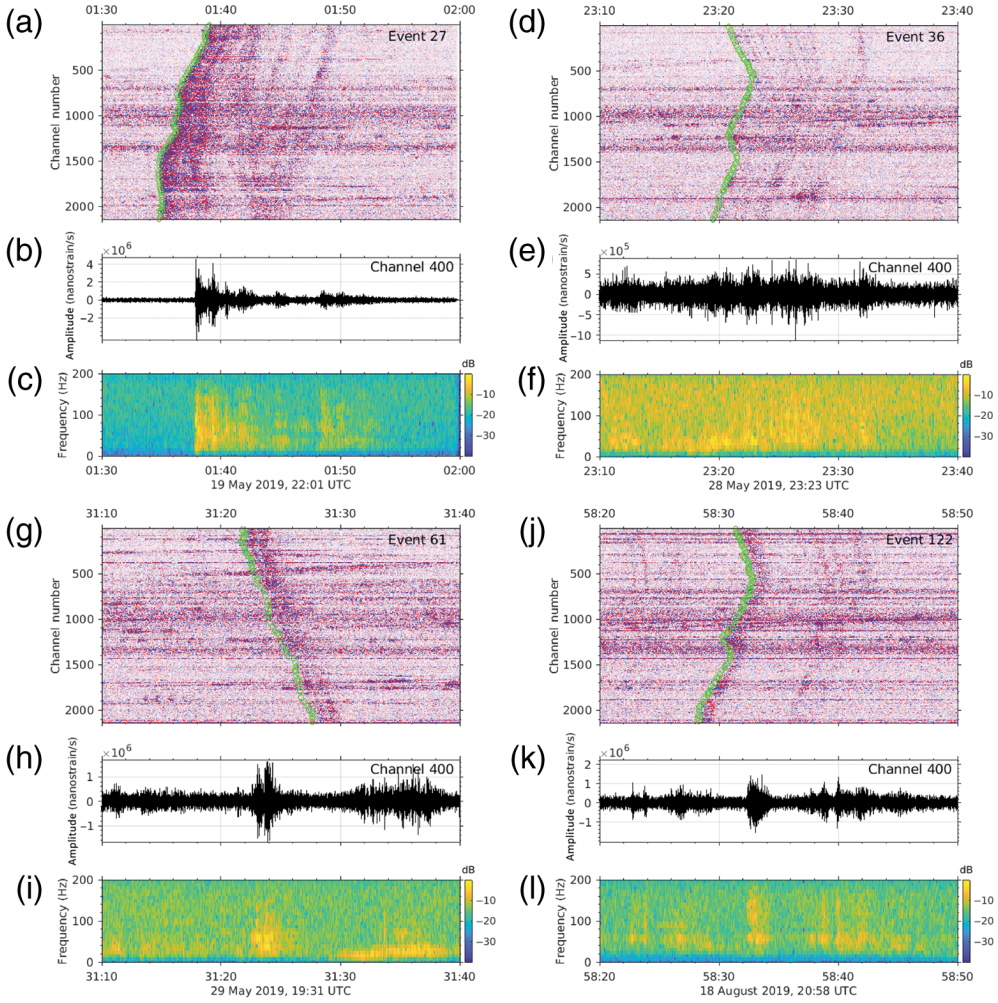


Figure 3. DAS records of four thunder events from 19, 28, and 29 May and 18 August, from top left to bottom right. Panels (a,d,g,j) show the event on all 2137 channels with manual picks shown in green, panels (b,e,h,k) show channel 400 from each event as a single trace, and panels (c,f,i,l) show a spectrogram of channel 400, illustrating the frequency content of the events. Events 27, 36, 61, and 122 are shown and have different offsets as well as varying numbers of claps. The color version of this figure is available only in the electronic edition.

event 61 must have a source location that minimizes the differences in arrival times between the kinks, which would be a point to the north or south at an equal angle relative to the northwest- and northeast-trending portions of the array. Also of interest, events 27, 36, and 122 all show multiple closely spaced arrivals with very similar offsets, probably indicating multiple thunderclaps, whereas event 61 contains one or at most two closely spaced arrivals. In all the shown events, each arrival tends to last ~2 s. In the spectrograms, we can see that the events tend to contain frequencies from 10 to 150 Hz, with attenuation of higher frequencies. Events 36 and 61 contain less of the high frequencies above 120 Hz, whereas event 122 lacks low frequencies below 20 Hz. These frequency values are consistent with previous values from acoustic studies of thunder (Lin and Langston, 2007). Variability of the frequency range between events could be due to a range of factors, including the intensity of the thunder, multiple claps versus single claps, and whether the thunder was caused by cloud-to-ground or cloud-to-ground lightning, which could change the orientation of the sound wavefront. The distance and direction to the source of the thunder also would have an effect due to attenuation of high frequencies from more distant sources and the directional sensitivity of the DAS array.

Because of the dense seismic data (Fig. 4), we can reconstruct the thunderquake wave propagation from two successive events. In the time sequence of Figure 4a–d, a thunderquake source excites at around channel 1700 (shown as a red star in Fig. 4a) and propagates outward along the fiber array. Given the assumption of a homogeneous subsurface medium, the wavefront of a thunderquake denoted by the green circle is illustrated. A sequent thunderquake event is illustrated in Figure 4e–h. Although the thunderquake source is away from the array, raw DAS data of this event provide insights into the wave-propagation direction from northwest to southeast and the wave complexity as the result of multiple wavefronts arriving in a sequence (perfect-circle wavefronts in a homogeneous medium). We believe that multiple wavefronts are likely caused by the interaction between return strokes of lightning strikes, which cause the thunderquake event (Zhu and Stensrud, 2019). Previous work has shown that the full waveform information enables us to locate the thunderquake source (Zhu and Stensrud, 2019). Further exploration of this wavefield is expected to allow us to study near-surface seismic properties using seismic tomography and interferometry.

Thunderstorm Location and Movement

Tracking thunderstorm movement using the DAS data requires a good grasp of the source location, and, to do this,

Downloaded from http://pubs.geoscienceworld.org/ssa/srl/article-pdf/doi/10.1785/0220200264/5276217/srl-2020264.1.pdf?casa_token=1-AImUXu6LMAAAAA:MKb73oRGMLD2ar73L2OqF-jelQ0EqtL7mYIlc1TycF5O5zVJmVsUHJV
by Pennsylvania State Univ Serials Dept, Tieyuan

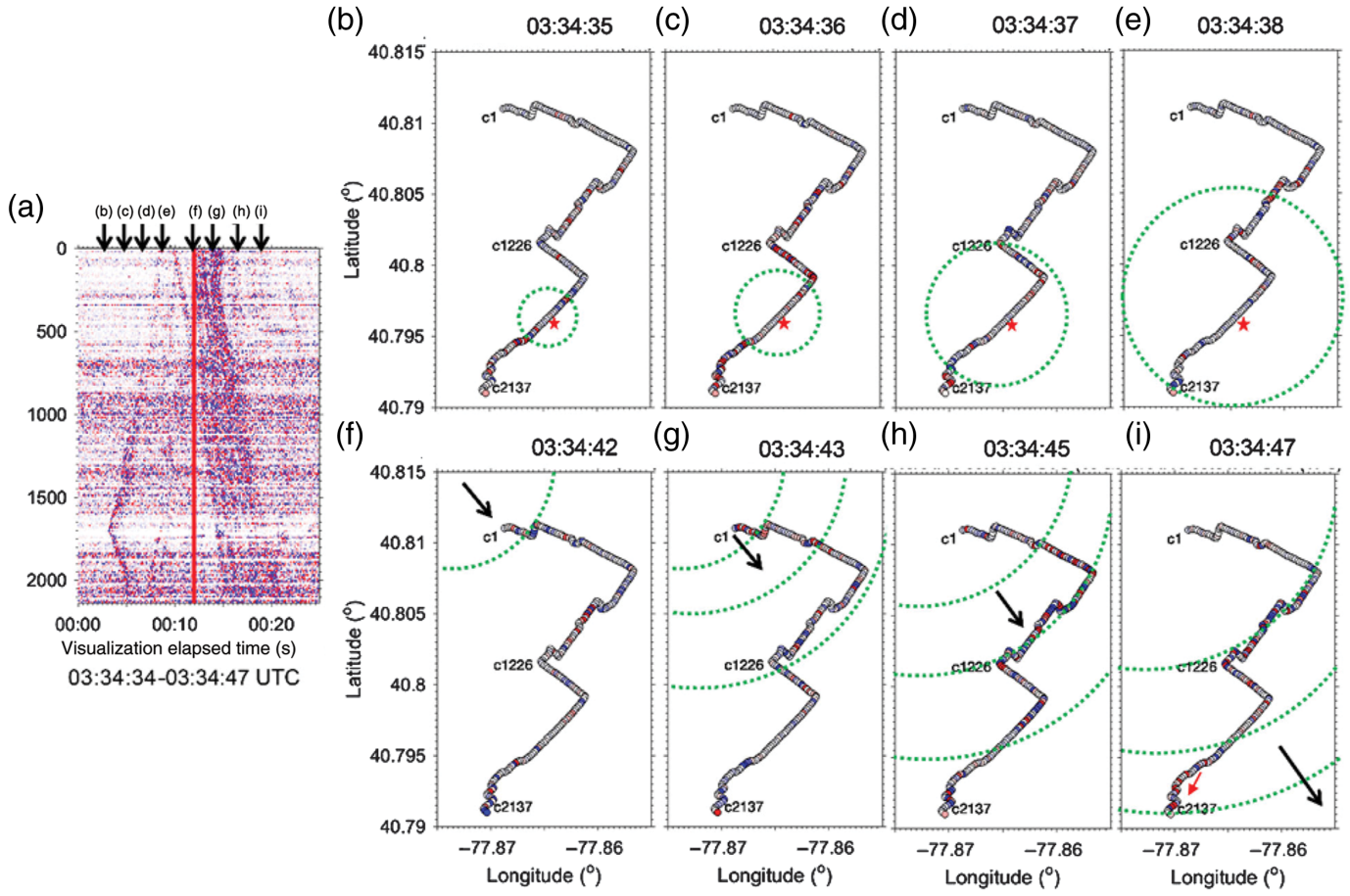


Figure 4. Snapshots of thunderquake wave propagation across the FORESEE array from two successive events (15 April 2019). Panels (b–i) correspond to elapsed times in panel (a). Red and blue colors showing in the fiber cable indicate the positive and negative amplitudes of the wave, respectively. Thunderquake DAS data (strain rate) in panel (a) were filtered from 1 to 200 Hz. In panels (f–i), the wave-propagation direction perpendicular to the wavefront is indicated by black arrows. The color version of this figure is available only in the electronic edition.

we must obtain approximate values for the back azimuth to the source and the propagation velocity and slowness. To get these values, we use the arrival times of each event as picked at all channels, to find the event back azimuth and apparent horizontal slowness using a time-domain grid-search technique (Lin and Langston, 2007).

In this method, we first calculate delay times at each sensor by subtracting the arrival time from a reference sensor. As a first approximation, we treat the acoustic wave generated by thunder as a plane wave and assume constant horizontal slowness for any given event. Using these assumptions, we can calculate hypothetical delay times for any set of apparent horizontal slowness and back azimuth, and minimize the residual between the hypothetical and observed delay times by searching a grid of these pairs. To estimate errors for the ray parameter and back azimuth, we apply a Monte Carlo error-propagation technique with a 2 s (±1 s) Gaussian random error to observed arrival times. For a more detailed description of this method, see Lin and Langston (2007). The result of the grid search is approximate values for the apparent horizontal slowness and back azimuth, which can be refined using another method.

We use a modified Geiger's method from Menke (2012), to calculate a more precise source location for the thunderquakes and to find their origin time. Geiger's method takes the apparent horizontal velocities from the grid search as a starting point and tests locations within a 20 × 20 km area of the fiber array, updating the source location and origin time to minimize the misfit between the observed and predicted arrival times. The sources are interpreted as occurring at the ground surface, so vertical components of the locations were minimized. Importantly, this method does not use the plane-wave assumption, making it more suitable for precise location of sources near the array.

Figure 5 shows example results from the grid-search method for event 27 on 19 May. The solution is the pair of slowness and azimuth, which minimizes the root mean square error between the observed (blue) and predicted (black) travel times, and is shown on the slowness versus azimuth plot in black. The predicted arrivals using Geiger's method are also shown (red), and, in the event shown, there is very little

Downloaded from http://pubs.geoscienceworld.org/ssa/srl/article-pdf/doi/10.1785/0220200264/5276217/srl-2020264.1.pdf?casa_token=1-AImUXu6LMAAAAA:MKb73oRGMLD2ar73L2OqF-jelQ0EqtL7mYIlc1TycF5O5zVJmVsUHJV
by Pennsylvania State Univ Serials Dept, Tievuan

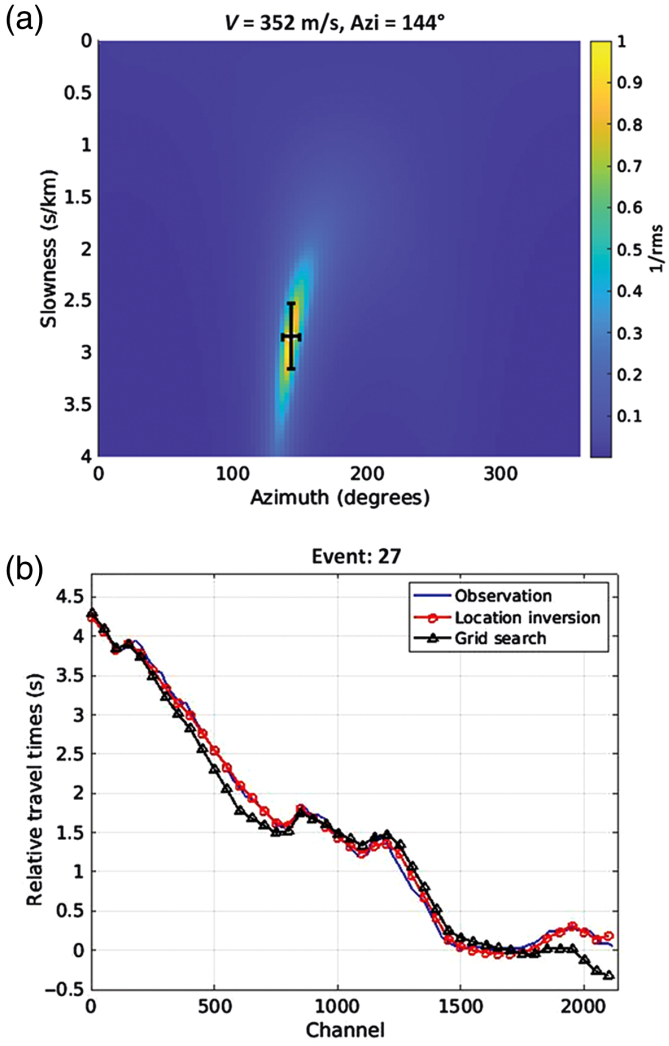


Figure 5. (a) A slowness versus azimuth plot from the grid search for event 27 from 19 May, color coded with the inverse root mean square (rms) error, with measurement error bars. The best solution is shown in black, and the best slowness and azimuth pair is displayed above the figure. (b) The manually picked travel times are shown (blue) and compared to the predicted times from the grid search (black) and Geiger's method (red). The close match between grid search and Geiger's method indicates the validity of the plane-wave assumption. The color version of this figure is available only in the electronic edition.

difference between the two methods. This suggests that the plane-wave assumption used in the grid search is relatively accurate in this case. The slowness and azimuth values obtained via grid search are plotted in Figure 6 for each date. The apparent horizontal velocities from the grid search range from 287 to 4167 m/s, with most falling between 300 and 500 m/s and error ranging from 17 to 1372 m/s (see Fig. 6 for plotted uncertainty). Interestingly, typical velocities are above the speed of sound (343 m/s), suggesting that the signal recorded is not primarily an air wave, which has implications for potential subsurface studies. Azimuth values from the grid search vary from 0° to 360° as would be expected, given thunderstorm movement and the randomness of lightning strikes. Typical uncertainties range from 4° to 18°, with a few points having an uncertainty as high as 180°. Large uncertainties in the slowness and azimuth are most likely due to either picking uncertainty (related to strength of signal or complex overprinting of multiple thunderquakes) or invalid model assumptions (plane-wave propagation, no vertical location component). The azimuth found via grid search is effectively an average azimuth for the whole array (as opposed to individual locations), which may provide another source of error.

Notably, although the slowness is lower for azimuths from about 60° to 120°, a trend that could be an indication of faster subsurface velocities to the east of the site, it is more likely an incidental result of less data from that direction, which is away from oncoming storms in the area. Contrary to expectation, the azimuths with their recording times do not map out a simple time progression tracking the movement of the thunderstorms, except for the 28 May data, which is too sparse to be thoroughly reliable. On 19 May, the time clustering in the data seems to suggest a movement direction perpendicular to the actual path of the storms, whereas on both 29 May and 18 August, no large-scale trend is obvious in Figure 6.

The source locations from Geiger's method were used to better interpret small-scale progressions in the data. The inverted source locations from Geiger's method for all dates (including 15 April, published previously) are shown in Figure 7. The locations are mostly to the west of State College, which is the direction from which most weather originates in the area, and they are concentrated in the valley with few near ridges. It is likely that the ridges have a limiting effect on the distance that surface waves can travel from the source. Source locations derived using this same methodology have been shown to match fairly well with recorded lightning strikes from the NLDN (Zhu and Stensrud, 2019).

Plotting the source locations from Geiger's method, according to their time of occurrence (Fig. 8), shows patterns markedly similar to Figure 6 but allows for a better geographic understanding of the results, aiding interpretation. Large-scale trends with the source times remain elusive, and the reason for this is twofold: first, thunderstorms in Pennsylvania are commonly scattered in their distribution at the local scale, which means that the events recorded by the DAS array for each date likely reflect the progress of several patches of storm instead of one large patch. Second, the apparently random incidence of lightning at any portion of the storm adds an additional complication to this tracking method.

In spite of these complications, several small trends can be seen in Figure 8. In Figure 8, on 19 May, three groups of events (blue, dark red, and red) are visible, suggesting three small patches of storm passed at slightly separated times, but so

Downloaded from http://pubs.geoscienceworld.org/ssa/srl/article-pdf/doi/10.1785/0220200264/5276217/srl-2020264.1.pdf?casa_token=1-AImUXu6LMAAAAA:MKb73oRGMLD2ar73L2OqF-jelQ0EqtL7mYIlc1TycF5O5zVJmVsUHJV
by Pennsylvania State Univ Serials Dept, Tieyuan

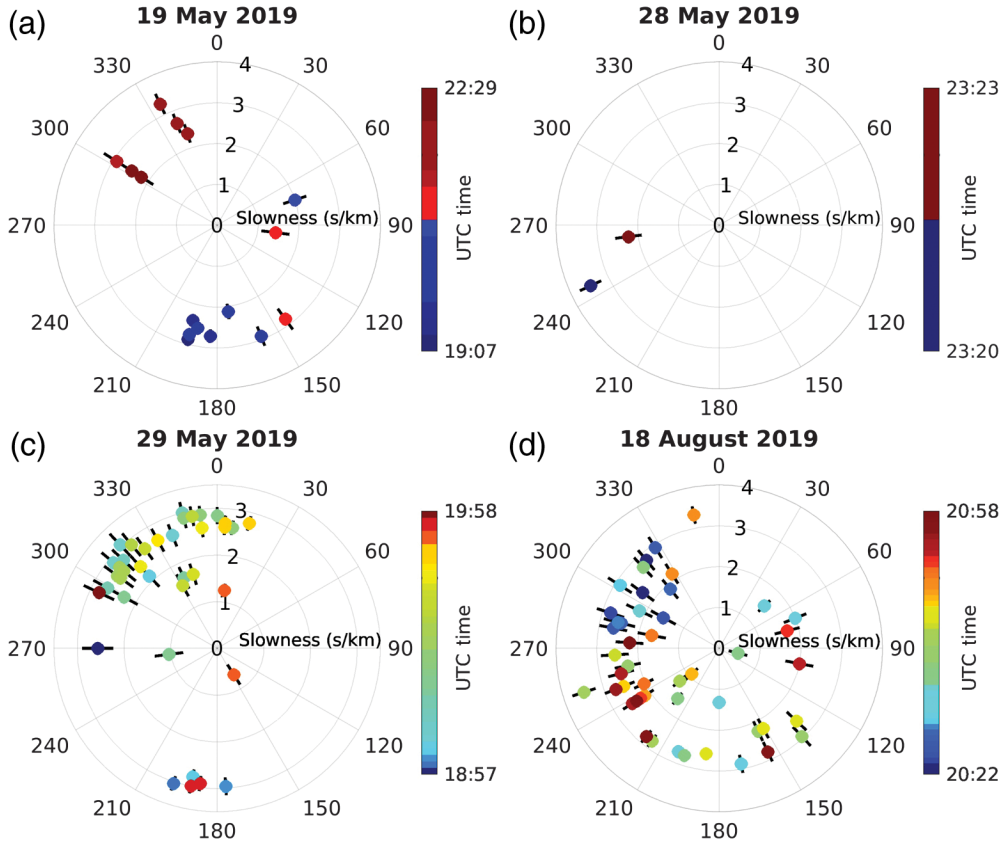


Figure 6. (a–d) Source azimuth and propagation slowness (radius value) obtained via the grid-search method for each date of interest. Slowness error bars are indicated in black. Each point is color coded to represent the time of detection by the DAS array. Points of adjacent colors show time progressions that correspond to thunderstorm movement, most notably on 18 August, blue to cyan colors. Points without a time progression indicate clusters of events very close in time corresponding to small patches of thunderstorm. The color version of this figure is available only in the electronic edition.

briefly that the events are very close to the same time, not revealing much about the propagation direction of the storms. On 28 May, only two samples are available, but they suggest a storm from the southwest, which matches weather records (Table 1). However, the sparsity of data limits the statistical credibility of that result.

Much more data are available for both 29 May and 18 August, and both show overlying sources from multiple patches of storm. Three groups or trends are visible on 29 May: blue, red to orange, and turquoise to green to yellow (Fig. 8). All three groups show a time progression from west to east, which roughly matches weather radar showing a series of small storms from the west-southwest (Table 1). Similarly, 18 August shows four trends, blue to cyan, green to yellow, orange to red, and dark red (Fig. 8). All except the last group show time progressions from the west-northwest, exactly corresponding to the recorded weather data (Table 1).

In Figure 9, the DAS location data for 29 May are directly compared to weather radar from the same date, obtained from Data and Resources. The local variation of the severity of this thunderstorm matches the times and locations of the DAS data. The first cluster of the storm (Fig. 9b) correlates with the blue–cyan portion of the data. The next portion of the storm arrives first north of State College (Fig. 9c) and then in a solid storm front extending from north to south. This matches the turquoise to green part of the data temporally, and, the thunderquake data also show sources to the north of the array, progressing from west to east, corresponding to the shape of the incoming storm front. The later red portion of the data is scattered, because the storm lacks strong fronts or structure at later times (Fig. 9d), which also could explain the lack of a time progression in the final cluster of data.

Discussion and Conclusions

In this article, we have shown conclusively that large dense DAS fiber-optic arrays can effectively record large numbers of thunderquakes with high signal-to-noise ratio, agreeing with previous results from Zhu and Stensrud (2019). The signal recorded shows characteristic frequencies from a few to 200 Hz, consistent with microphone studies of thunder and can be used to derive information regarding the azimuth and location of the source, and the horizontal propagation slowness and velocity of the ground-coupled wave.

The nature of the ground-coupled wave depends on the thunder source as well as how the waves are recorded by the DAS array, which is complicated by the single-component nature of the array and the directional sensitivity of the fiber. Kappus and Vernon (1991) found primarily vertical ground motion generated by thunderquakes, and the surficial nature of the thunder source and receiver suggests that the signal is dominated by surface waves. Furthermore, Lin and Langston (2007) found evidence in thunder data of retrograde elliptical particle motion consistent with locked Rayleigh waves. Love waves are also likely present, but the two phases cannot be effectively distinguished here because of the single-component fiber.

Downloaded from http://pubs.geoscienceworld.org/ssa/srl/article-pdf/doi/10.1785/0220200264/5276217/srl-2020264.1.pdf?casa_token=1-AImUXu6LMAAAAA:MKb73oRGMLD2ar73L2OqF-jelQ0EqtL7mYIlc1TycF5O5zVJmVsUHJV
by Pennsylvania State Univ Serials Dept, Tieyuan

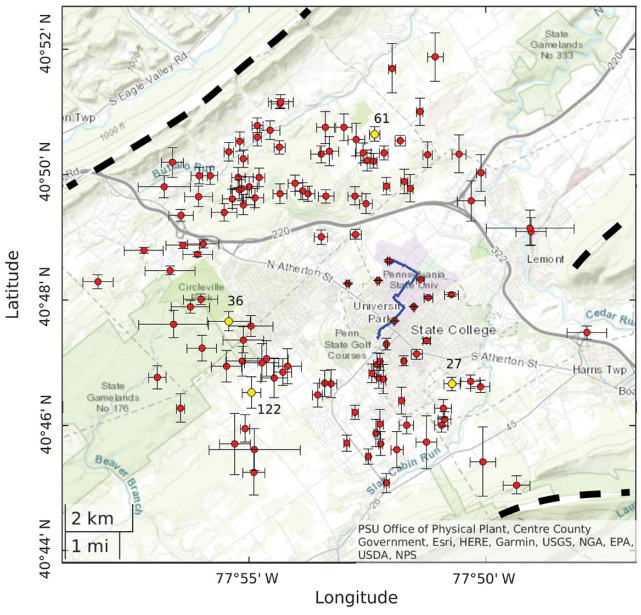


Figure 7. DAS array (shown in blue) along with source locations (red) derived from Geiger's method, neglecting the vertical component. Locations for the example events (Fig. 3), are shown in yellow and numbered, and ridgelines are outlined by black-dashed lines. The events are clustered within the valley with more to the west and northwest, the predominant weather direction. The color version of this figure is available only in the electronic edition.

The fiber is most sensitive to Rayleigh waves propagating parallel to the fiber and Love waves traveling at a 45° angle (Kuvshinov, 2015), which may have the effect of camouflaging amplitude minima for sources that excite motion at 90° to large portions of the array. Because of this difficulty, we assume, generally, that the first arrivals picked for the events are surface waves, and may be mixed Rayleigh and Love waves. Further studies will focus on phase discrimination to shed light on this important question.

The shapes and source parameters of thunder events reveal a great deal about the nature of the thunderstorm source. Multiple arrivals in the DAS data indicate multiple claps of thunder likely due to return strokes in the lightning channel (Dwyer and Uman, 2014). The source locations found via Geiger's method locate individual lighting events, and, when correlated with time trace out the path of thunderstorms, effectively allowing for seismic real-time tracking of atmospheric events at the local scale. It may also be possible that DAS records can distinguish between cloud-to-ground and cloud-to-cloud lightning strikes, using the propagation velocity. Waves from cloud-to-ground strikes are thought to propagate as a surface wave through the shallow subsurface for the majority of their travel path, whereas waves from cloud-to-cloud lightning will likely remain in the air before contacting the ground near the sensor. This difference in propagation would be reflected in the velocity of the first arrival, with velocities near the speed of sound (343 m/s) possibly indicating cloud-to-cloud lightning. Velocity data do show some events with velocities close to the speed of sound, whereas others have much higher or lower velocities, but, due to some overlap between surface-wave and sound-wave velocities, further study is needed to confirm the distinction in the source type. Correlating velocity with the z component of source locations may be revealing toward this end. Future work may also depart from the point-source approximation and be able to trace horizontal components in lightning paths using polarization analysis, similar to work done with seismometers (Kappus and Vernon, 1991).

The propagation path of the waves from thunder also has implications for subsurface studies. Lin and Langston (2007) showed that thunder-induced ground motions may often propagate in the near surface as air-coupled Rayleigh

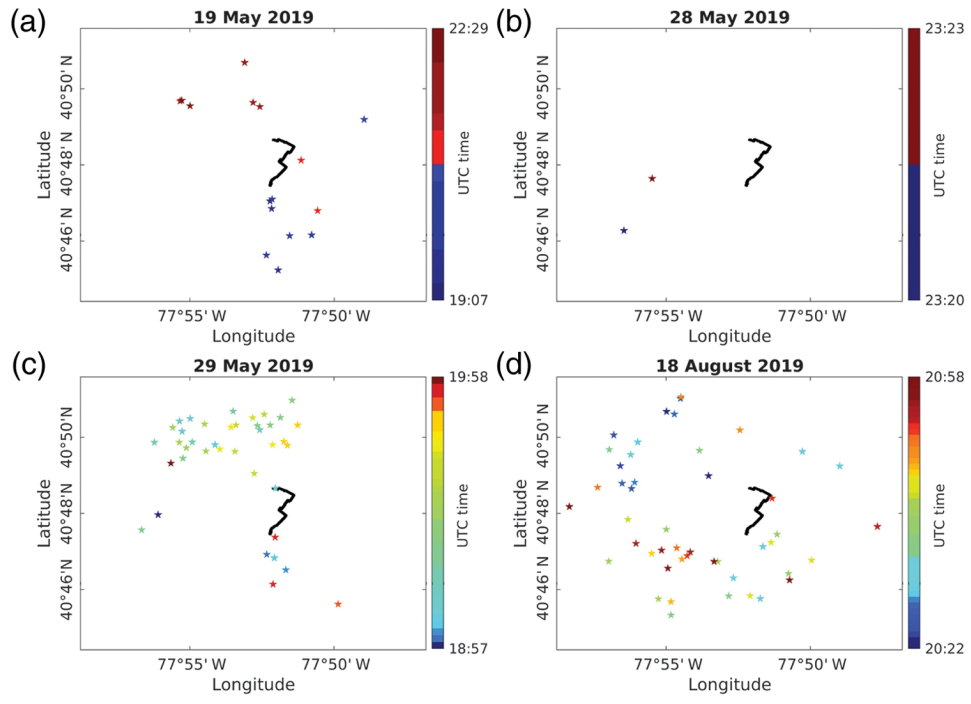


Figure 8. (a–d) Plots of event-source locations from each date found with Geiger's method and color coded with the time that each event was recorded by the DAS array. Each date shows clusters of events around specific times, which correspond to patches of thunderstorm passing near the array. Events near each other in time follow a track generally from west to east, recording the progress of the thunderstorms. The color version of this figure is available only in the electronic edition.

Downloaded from http://pubs.geoscienceworld.org/ssa/srl/article-pdf/doi/10.1785/0220200264/5276217/srl-2020264.1.pdf?casa_token=1-AImUXu6LMAAAAA:MKb73oRGMLD2ar73L2OqF-jelQ0EqtL7mYIlc1TycF5O5zVJmVsUHJV
by Pennsylvania State Univ Serials Dept, Tieyuan

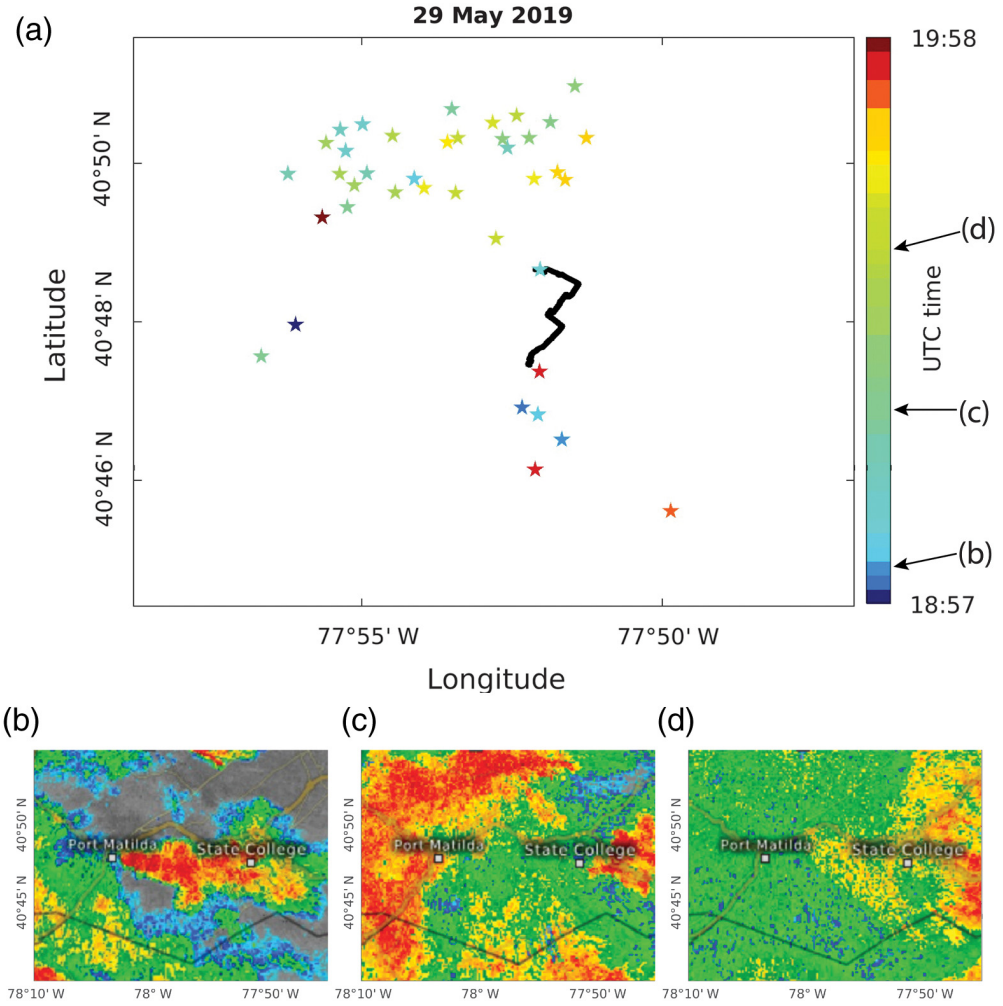


Figure 9. Source locations from (a) 29 May compared to weather radar (showing base reflectivity, Data and Resources) from the same date, at times, (b) 19:01:30, (c) 19:21:13, and (d) 19:41:16 UTC. The fiber-optic array is located at the labeled position of State College on the radar maps. The event time, as indicated by the color bar, is approximately linked to corresponding patches of storm on the radar by the arrows. The color version of this figure is available only in the electronic edition.

waves. Zhu and Stensrud (2019) further used forward seismic modeling to simulate *SH* waveforms to fit observed thunder-induced surface waves recorded by DAS, given a layered *SH* velocity model estimated from Geiger's method. Lin and Langston (2009b) proposed, using these signals, to constrain near-surface velocity structure. In cases in which the propagation path of the wave is mostly in the near surface (not an air wave), it will contain much information about the near-surface structure. Future work will investigate the possibility of using surface-wave tomography, to find near-surface velocity structure on the local to regional scale near State College, Pennsylvania, in favor of the well-distributed sources around the local area (Fig. 8). Compared to ambient-noise virtual sources that are often used in a similar context in areas lacking in seismic activity, these thunderquake sources are powerful with a distinct phase to be picked; because of high frequencies (a few to 100 Hz), the thunderquake data could potentially provide very high resolution velocity maps in the local scale. A thunderstorm-based method, if successful, would have many applications in areas with little seismic activity but many thunderstorms, especially the eastern United States. Urban areas, in particular, would benefit, having many fiber-optic cables available for use as DAS arrays, and much need for near-surface characterization for engineering and hazard assessment.

Although many useful applications exist for thunderquake data recorded by DAS arrays, one challenge is the sheer volume of data, which renders manual location of useful signals and distinguishing thunder from earthquakes and ambient noise very time intensive. Smart (e.g., machine learning) algorithms present an attractive alternative to facilitate timely data mining and lead to faster analysis of results (Li and Zhan, 2018; Martin *et al.*, 2018; Jakkampudi *et al.*, 2020). If analysis of DAS data from thunderstorms can be effectively streamlined, it could lead to an improved understanding of atmospheric effects on the subsurface, a new viable seismic source, and effective tracking of thunderstorms and lightning activity at local scales.

Data and Resources

The distributed acoustic sensing (DAS) data for this project were obtained using the Penn State Fiber Optic foR Environmental SEnsEing (FORESEE) array in State College. The downsampled DAS data used in this project will be available at sites.psu.edu/tzhu/foresee (last accessed October 2020). Broadband seismic waveform data for the PSRS seismic station were retrieved from the Incorporated Research Institutions for Seismology (IRIS) Data Management Center (last accessed July 2020). Past weather information for data-mining purposes was obtained from Timeanddate.com (last accessed July 2020) and Weather.us (last accessed July 2020), as well as Doppler radar that aided in data analysis. Both of these weather databases are freely available to the public. The approximate

Downloaded from http://pubs.geoscienceworld.org/ssa/srl/article-pdf/doi/10.1785/0220200264/5276217/srl-2020264.1.pdf?casa_token=1-AImUXu6LMAAAAA:MKb73oRGMLD2ar73L2OqF-jelQ0EqtL7mYIlc1TycF5O5zVJmVsUHJV
by Pennsylvania State Univ Serials Dept, Tieyuan

direction of origin for each thunderstorm was determined independently from the DAS data by inspecting weather radar from the website weather.us/radar-us (last accessed December 2020). MATLAB is available at www.mathworks.com/products/matlab (last accessed January 2021).

Declaration of Competing Interests

The authors acknowledge that there are no conflicts of interest recorded.

Acknowledgments

The authors thank Todd Myers and Ken Miller at Penn State, and Thomas Coleman from Silixa for their help setting up the distributed acoustic sensing (DAS) array at Penn State. The authors also thank Eileen Martin for help with project planning and tap tests, and Chuck Ammon and Sridhar Anandakrishnan for their feedback on the project concept. The authors also appreciate the entire Environmental Geophysics Research Group at Penn State for their invaluable support and feedback in the course of this project. This project is supported by a seed grant from the Penn State Institutes of Energy and the Environment and the Institute of Natural Gas Research.

References

Cummins, K. L., E. P. Krider, and M. D. Malone (1998). The U.S. national lightning detection network™ and applications of cloud-to-ground lightning data by electric power utilities, *IEEE Trans. Electromagn. Compat.* **40,** 465–480.

Dwyer, J. R., and M. A. Uman (2014). The physics of lightning, *Phys. Rep.* **534,** 147–241.

Ebeling, C. W., and S. A. Stein (2011). Seismological identification and characterization of a large hurricane, *Bull. Seismol. Soc. Am.* **101,** 399–403.

Jakkampudi, S., J. Shen, W. Li, A. Dev, E. R. Martin, and T. Zhu (2020). Footstep detection in urban seismic data with a convolutional neural network, *The Leading Edge* **39,** 654–660.

Kanamori, H., J. Morit, D. L. Anderson, and T. H. Heaton (1991). Seismic excitation by the space shuttle Columbia, *Nature* **349,** 781–782.

Kappus, M. E., and F. L. Vernon (1991). Acoustic signature of thunder from seismic records, *J. Geophys. Res.* **96,** 10,989.

Kuvshinov, B. N. (2015). Interaction of helically wound fibre-optic cables with plane seismic waves, *Geophys. Prospect.* **64,** 671–688.

Langston, C. A. (2004). Seismic ground motions from a bolide shock wave, *J. Geophys. Res.***109,** 1–23.

Li, Z., and Z. Zhan (2018). Pushing the limit of earthquake detection with distributed acoustic sensing and template matching: A case study at the Brady geothermal field, *Geophys. J. Int.* **215,** 1583–1593.

Lin, T. L., and C. A. Langston (2006). Anomalous acoustic signals recorded by the CERI seismic network, *Seismol. Res. Lett.* **77,** 572–581.

Lin, T. L., and C. A. Langston (2007). Infrasound from thunder: A natural seismic source, *Geophys. Res. Lett.* **34,** 1–6.

Lin, T. L., and C. A. Langston (2009a). Thunder-induced ground motions: 1. Observations, *J. Geophys. Res.* **114,** 1–19.

Lin, T. L., and C. A. Langston (2009b). Thunder-induced ground motions: 2. Site characterization, *J. Geophys. Res.* **114,** 1–11.

Martin, E. R., C. M. Castillo, S. Cole, P. S. Sawasdee, S. Yuan, R. Clapp, M. Karrenbach, and B. L. Biondi (2017). Seismic monitoring leveraging existing telecom infrastructure at the SDASA: Active, passive, and ambient-noise analysis, *The Leading Edge* **36,** 1025–1031.

Martin, E. R., F. Huot, Y. Ma, R. Cieplicki, S. Cole, M. Karrenbach, and B. L. Biondi (2018). A seismic shift in scalable acquisition demands new processing: Fiber-optic seismic signal retrieval in urban areas with unsupervised learning for coherent noise removal, *IEEE Signal Process. Mag.* **35,** 31–40.

Menke, W. (2012). *Geophysical Data Analysis: Discrete Inverse Theory*, Elsevier/Academic Press, Amsterdam, The Netherlands, 163–188.

Rudlosky, S. D., S. J. Goodman, K. S. Virts, and E. C. Bruning (2019). Initial geostationary lightning mapper observations, *Geophys. Res. Lett.* **46,** 1097–1104.

Voss, P. H., T. Dahl-Jensen, and T. B. Larsen (2015). Acoustic events on a small seismological network—Shock waves from thunder and fireballs, *Geol. Surv. Denmark Greenl. Bull.* **33,** 25–28.

Zhu, T., and D. J. Stensrud (2019). Characterizing thunder-induced ground motions using fiber-optic distributed acoustic sensing array, *J. Geophys. Res. Atmos.* **124,** 12,810–12,823.

Zhu, T., J. Shen, and E. R. Martin (2021). Sensing earth and environment dynamics by telecommunication fiber-optic sensors: An urban experiment in Pennsylvania USA, *Solid Earth* **12,** 219–235.

Manuscript received 31 July 2020
Published online 24 March 2021

Downloaded from http://pubs.geoscienceworld.org/ssa/srl/article-pdf/doi/10.1785/0220200264/5276217/srl-2020264.1.pdf?casa_token=1-AImUXu6LMAAAAA:MKb73oRGMLD2ar73L2OqF-jelQ0EqtL7mYIlc1TycF5O5zVJmVsUHJV
by Pennsylvania State Univ Serials Dept, Tieyuan